MedChemComm

RESEARCH ARTICLE

View Article Online
View Journal | View Issue

Cite this: *Med. Chem. Commun.*, 2019, **10**, 2102

Radioiodinated 9-fluorenone derivatives for imaging α7-nicotinic acetylcholine receptors†

Hang Gao, Shuxia Wang, Bingchao Qiang, Sixuan Wang and Huabei Zhang*

Received 27th August 2019,
Accepted 14th October 2019

DOI: 10.1039/c9md00415g

rsc.li/medchemcomm

A series of 9*H*-fluoren-9-one substituents were synthesized and evaluated for imaging cerebral α7-nAChRs. *Meta*-iodine substituted 9-fluorenone **5** with high binding affinity (K_i = 9.3 nM) and selectivity was radiolabeled with ^{125}I. Fully *in vitro* and *in vivo* studies of [^{125}I]**5** have been performed. [^{125}I]**5** exhibited well brain uptake with a peak concentration of 7.5 ± 0.9% ID/g in mice brains. Moreover, *ex vivo* autoradiography studies and micro single-photon emission computed tomography (micro-SPECT/CT) dynamic imaging in mice confirmed its *in vivo* imaging properties. Besides, molecular docking and MD studies were also performed to interpret the binding mechanisms of the two series of ligands towards α7-nAChRs. To conclude, the *meta*-iodine substituted 9-fluorenone [^{125}I]**5** could be a promising tracer for imaging α7-nAChRs.

Introduction

The nicotinic acetylcholine receptors (nAChRs), which are related to the neurotransmitter acetylcholine (ACh), are classified into neuronal type (α2–α10 and β2–β4) and muscle type (α1, β1, γ, δ and ε) receptors.[1] nAChRs in humans are ligand-gated ion channels and can assemble into different subtypes.[2] In human brains, the homomeric α7 and heteromeric α4β2 nicotinic receptor subtypes are predominant among other nAChR subtypes.[3]

It is clear that nicotine has a high binding affinity to the α4β2 subtype, but a much lower affinity to α7-nAChRs. Due to their unique structure, the α7-nAChRs exhibit the fastest desensitization kinetics of all nAChRs and display a strong binding to methyllycaconitine (MLA) or α-bungarotoxin (α-Bgt).[4] The α7-nAChRs have high permeability to calcium and are expressed in various cells in the brain. In human cerebral cortical neurons, astrocytes, microglia, oligodendrocyte precursor cells and endothelial cells, the α7-nAChRs exhibited their own roles in regulating physiology such as learning, memory, sensorimotor gating and even inflammation.[5–10] Further studies illustrated that α7-nAChRs have been involved in numerous brain disorders including schizophrenia (SCZ), Alzheimer's disease (AD), anxiety, bipolar disorder and traumatic brain injury.[11–14]

With an intensive progress of neurophysiology, the α7-nAChR emerged as a promising therapeutic target for psychiatric disorders. Preclinical and early clinical studies showed that α7-nAChR partial agonists displayed promising results for the treatment of neurodegenerative diseases.[15–17] However, postmortem studies in AD and SCZ patients showed a loss of α7-nAChRs in their human cerebral tissues.[18] The suppression of inflammation may be a key point that could protect these receptors in brain pathologies, but the physiological and pharmacological roles of the α7-nAChRs in CNS remained unclear.[19–22] Even so, several selective α7-nAChR partial agonists have reached clinical trials such as GTS-21, TC-5619 and EVP-6124.[23–25] Unfortunately, the invalid cases of planned therapies occurred beyond the expected results and a loss of drug effect was observed when increasing the dose of agonists above the threshold.[24,26,27] Therefore, it is urgently needed to develop α7-nAChR biomarkers *in vivo* to make early diagnosis of neurodegenerative diseases and to evaluate the efficiency of such therapies.

The *in vivo* imaging and quantifying of α7-nAChRs with positron emission tomography (PET) and single-photon emission computed tomography (SPECT) techniques may be of paramount importance to answer the questions. In the past few years, many radiotracers targeted to α7-nAChRs have been developed and tested on non-primates, but most have suboptimal character to do further research on humans. For the ^{11}C and ^{18}F labelled PET tracers, various basic structures have been developed such as 1,4-diazabicyclo[3.2.2.]nonane derivatives like [^{11}C]CHIBA-1001,[28] spirofuropyridine derivatives like [^{18}F]AZ11637326,[29] fluorinated derivatives of dibenzo[*b*,*d*]thiophendioxide like [^{18}F]ASEM and [^{18}F]

Key Laboratory of Radiopharmaceuticals of Ministry of Education, College of Chemistry, Beijing Normal University, Beijing 100875, China.
E-mail: hbzhang@bnu.edu.cn

† Electronic supplementary information (ESI) available. See DOI: 10.1039/c9md00415g

DBT10,[30] and newly discovered 9*H*-fluoren-9-one substituted derivative [^{18}F]**1**.[31,32] As for the ^{123}I and ^{125}I labelled SPECT radiotracers, [^{125}I]iodo-ASEM showed promising results yet lacked some *in vivo* studies (Fig. 1).[33]

In this study, we describe a series of 9*H*-fluoren-9-one substituted derivatives with high to moderate binding affinities towards α7-nAChRs. *Meta*-iodine substituted 9-fluorenone [^{125}I]**5** had an improvement on yields of radiolabelling and is biologically equivalent to *ortho*-iodine substituted. [^{125}I]**5** could serve as a promising radiotracer for imaging α7-nAChRs. In addition, the study of synthesized amino and fluorinated substituents together with molecular modeling would provide some help in designing new α7-nAChR ligands.

Results and discussion

Chemistry

The synthesis routes of the *meta*-substitution of compounds **3**, **4**, and **5** are shown in Scheme 1. The nonlabelled precursor **4** started from 2,7-dibromo-9*H*-fluoren-9-one (**2**). The "one-arm" substituted **3** was synthesised with a chemical quantity of 0.9 eq. of 1,4-diazabicyclo[3.2.2]nonane *via* the Buchwald–Hartwig Pd-catalyzed cross-coupling reaction. The nonlabelled precursor **4** was prepared from **3** in anhydrous toluene catalyzed by $Pd(PPh_3)_4$. The final nonradioactive **5** was easily prepared with iodine and dichloromethane at R.T. in high yields.

The synthesis of 4-methylpiperazin-1-yl substituted derivatives started from **6**. Fluoranthene **6** was oxidized by chromium(VI) oxide to open the loop to afford carboxylic acid **7** in a high yield. Carboxylic acid **7** was brominated into **8** and further produced Boc-protected aniline **9** by the Curtius rearrangement through a one pot reaction. The Boc-protecting group of **9** was removed with diluted hydrochloric acid to obtain **14**. After the Schiemann reaction, fluorine substituted **15** was generated. The final derivatives **10**, **11**, **16** and **17**, were prepared by the Buchwald–Hartwig cross-coupling reaction between the nitrogen heterocyclic rings and **9** or **15** respectively. It's worth mentioning that in the procedure of the Buchwald–Hartwig cross-coupling reaction, the total yields *k* of **16–18** decreased due to the existence of the fluorine atom on **15**, which was the same as what Teodoro reported.[32] The fluorine atom may act as a leaving group that leads to the low selectivity of cross-coupling reactions and bring difficulties in the separation and purification of these compounds.

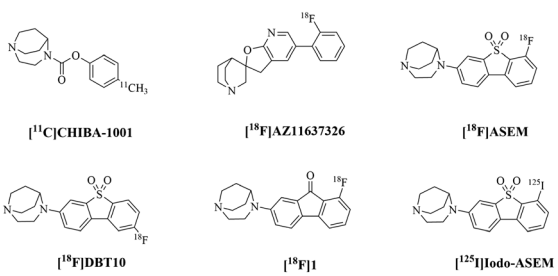

Fig. 1 Reported α7-nAChRs radiotracers.

In vitro binding assay

The *in vitro* binding affinities of α7-nAChRs and selectivity to homologous α4β2 subtype were measured, respectively. Rat cortical membranes were used to conduct the binding assays. 0.4 nM [^{125}I]α-bungarotoxin ([^{125}I]α-Bgt) was used as a competitor to have a K_d value of 0.7 nM.[34] Besides, the binding affinity of the specific α7-nAChR antagonist methyllycaconitine (MLA) was also measured under the same conditions as the reference compound to ensure the reliability of the method.[35]

As shown in Table 1, among all the tested compounds, 1,4-diazabicyclo[3.2.2]nonan-4-yl substituted **3** and **5** showed a strong affinity (K_i = 9.3 nM) toward the α7-nAChRs and are at the same level as iodo-ASEM. Precursor **4** was found to suffer an obvious decrease of affinity (K_i > 500 nM), which may be caused by the steric bulk of the tributylstannyl group. The 4-methylpiperazin-1-yl substituted fluoren-9-ones manifested moderate affinities compared to 1,4-diazabicyclo[3.2.2]nonane substituent **5**, which indicates that the heterocyclic nitrogen groups are crucial to obtain binding affinities. Among **10–18**, amino substituents **12** and **13** were found to have higher binding affinities than the fluoro substituted compounds, which indicates that a connection between ligands and proteins may exist. The affinities of piperazin-1-yl substituents **13** and **18** were higher than 4-methylpiperazin-1-yl substituents **12** and **16** respectively.

The selectivity to heteromeric α4β2-nAChRs was also determined using [^{3}H]cytisine (1 nM) as a competing radioligand.[36] All the tested compounds were found to have relatively lower affinities to α4β2-nAChRs. *Meta*-iodine-substituted **5** exhibited good selectivity.

Radiochemistry

5, which had a high binding affinity within the series, was chosen to be radiolabelled with ^{125}I in a high yield route (Scheme 2). Compound [^{125}I]**5** was prepared from its corresponding hexabutylditin precursor **4** through an iododestannylation reaction using hydrogen peroxide as an oxidant with a high radiochemical yield of 85.4%. Compared to iodo-ASEM, the efficiency of radiolabelling was greatly improved, which made it easier to use [^{125}I]**5** in some ways. [^{125}I]**5** was eluted at 50.871 min and obtained with a radiochemical purity of greater than 98% after solid-phase extraction as shown in Fig. 2. The final radiochemical identification of radioiodinated ligand [^{125}I]**5** was verified by coinjection with a nonradioactive compound **5** using HPLC profiles. [^{125}I]**5** has a retention time of 8.311 min compared to 8.004 min of **5**.

In vitro stability study

The *in vitro* stability of [^{125}I]**5** in fetal bovine serum and saline were determined separately. Highly purified [^{125}I]**5**

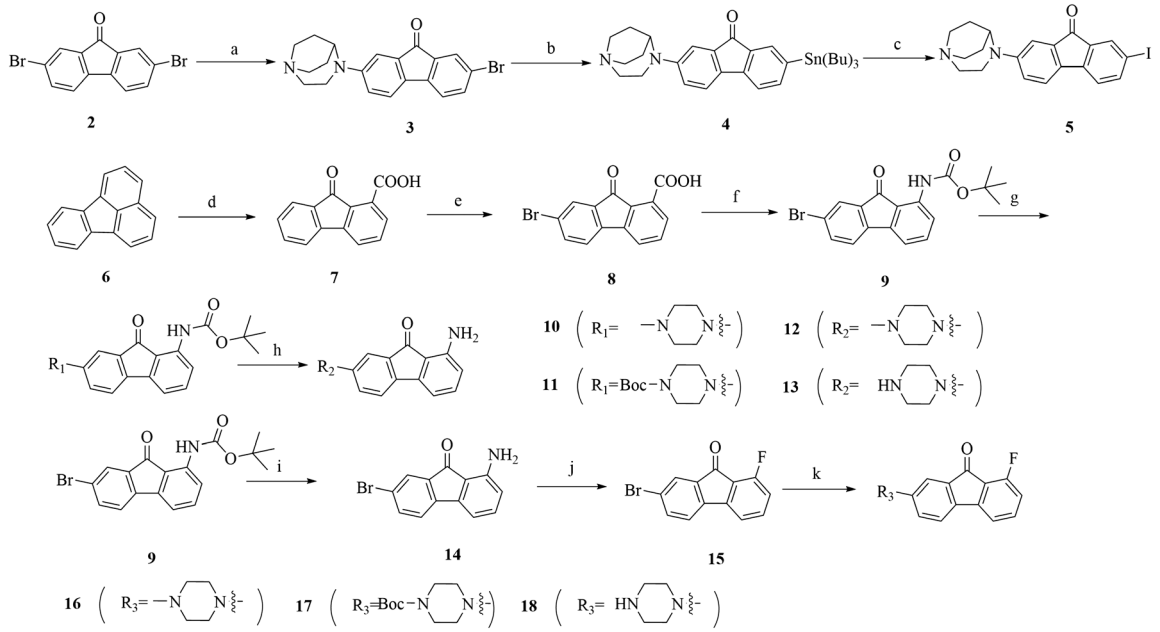

Scheme 1 Reagents and conditions: (a) Cs_2CO_3, $Pd_2(dba)_3$, BINAP, toluene, 80 °C, 51.6% yield; (b) $Pd(PPh_3)_4$, $Sn_2(Bu)_6$, toluene, 120 °C, 37.4% yield; (c) I_2, CH_2Cl_2, $NaHSO_3$. R.T., 58.3% yield; (d) CrO_3, H_2O, CH_3COOH, 80–85 °C, 110–120 °C, 66.1% yield; (e) Br_2, 80–85 °C, 96.5% yield; (f) Et_3N, DPPA, *t*-BuOH, toluene, 110 °C, 73.0% yield; (g and k) Cs_2CO_3, $Pd(dba)_3$, BINAP, toluene, 85 °C, 34.6–67.2% yield; (h and i) CH_3CN, 1 N HCl, 80 °C, 1 N NaOH, 78.9–84.5% yield; (j) HBF_4, 0–5 °C; $NaNO_2$; H_2O, 120 °C, 33.4% yield.

were hatched at 37 °C and R.T., respectively, for 1–12 hours. The radiochemical purity of the miscible liquids was determined *via* HPLC. The results showed that the radiochemical purity of [^{125}I]**5** remained greater than 98% both in serum and saline (Fig. 3). The results demonstrated that [^{125}I]**5** has a high *in vitro* biostability in a simulated physiological environment.

Biodistribution in tissues and organs of mice

The biodistribution studies of [^{125}I]**5** were conducted on normal Kunming mice (female, 18–22 g). Radioiodinated [^{125}I]**5** showed a rapid brain uptake of 4.2 ± 0.2% ID g^{-1} at 5 min of post-injection (Table 2). The peak concentration of [^{125}I]**5** in the brain was 7.5 ± 0.9% ID g^{-1} at 30 min, then gradually dropped to 4.6 ± 0.5% ID g^{-1} at 60 min. The brain$_{30\ min}$/brain$_{120min}$ was 2.7, presenting a good clearance rate for brain imaging. Among the peripheral organs, the lungs exhibited an exceptional absorption of 49.8 ± 9.2% ID g^{-1} at 5 min and also a fast clearance. The organs of liver and kidney showed moderate radioactive uptake, probably due to the metabolism of these organs. The thyroid showed a relatively low uptake within 60 min, indicating the good stability of the iodide group *in vivo*. The highest brain/blood ratio was 8.3 at 30 min, which illustrated good properties of [^{125}I]**5** in SPECT/CT imaging studies.

Table 1 *In vitro* binding affinities (K_i, nM) of MLA, nicotine, **3**, **5**, **12**, **13**, **16** and **18** toward α7-nAChR and α4β2 subtypes

Compd	K_i (nM) α7[a]	K_i (nM) α4β2[b]	Selectivity α7/α4β2
MLA	2.7 ± 0.9	nt[c]	
Nicotine	nt[c]	3.8 ± 1.2	
3	1.9 ± 0.3	2036 ± 446	1088
5	9.3 ± 0.4	4975 ± 578	537
12	224 ± 13	>10 000	
13	186 ± 9	9211 ± 314	50
16	521 ± 55	>10 000	
18	207 ± 10	8254 ± 452	40

[a] SD rat (female, 180–270 g) cerebral cortex; radiotracer, [^{125}I]α-Bgt (0.4 nM), K_d = 0.7 nM; K_i values are the mean ± SD of assays performed in triplicate. [b] SD rat (female, 180–270 g) cerebral cortex; radiotracer, [^{3}H]cytisine (1 nM), K_d = 0.77 nM; K_i values are the mean ± SD of assays performed in triplicate. [c] nt: not tested.

Biodistribution of brain regions in mice

The brain region distribution studies of [^{125}I]**5** were performed on Kunming mice to test the dynamic binding properties under the physiological level (Fig. 4). In a few minutes of tail vein injection, [^{125}I]**5** exhibited rapid initial brain uptake. The peak concentration in the brain was appeared at 30 min, followed by a moderate washout. A higher radioactive accumulation of [^{125}I]**5** appeared in the frontal cortex, hippocampus, superior/inferior colliculus

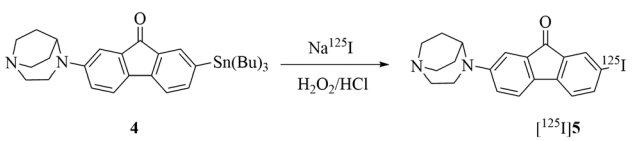

Scheme 2 Radiosynthesis of [^{125}I]**5**.

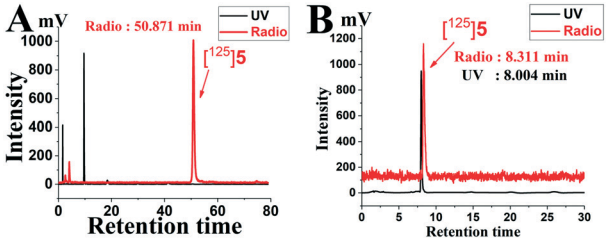

Fig. 2 (A) HPLC chromatogram of the preparation of [^{125}I]**5**. (B) Coinjection of [^{125}I]**5** and **5**.

and striatum. In the frontal cortex of the brain, [^{125}I]**5** exhibited the highest value of 6.6 ± 0.5% ID g^{-1} at 30 min. The hippocampus had the second-ranked uptake of 5.9 ± 0.4% ID g^{-1} at 30 min and a slower clearance. The uptakes of the superior/inferior colliculus and striatum were relatively lower, 5.3 ± 0.4% ID g^{-1} and 4.5 ± 0.3% ID g^{-1} at 15 min respectively. The cerebellum had the lowest uptake. The distribution of [^{125}I]**5** were in accordance with the biodistribution of α7-nAChRs in rodents.[37]

Blockade studies

To ensure the specificity of the radiotracer under physiological conditions, self-blockade studies with a non-labelled standard **5** were studied on Kunming mice. An obvious reduction of radioactive accumulation among all regions in the mice cerebellum was observed, which indicated a successful blockade of the ligand in the mice brain. The frontal cortex, hippocampus and superior/inferior colliculus of the brain have a blockade ratio of 66.9%, 85.1% and 80.1%, respectively (Fig. 5A). The blockade ratio of the cerebellum is less than 40%, indicated that the uptake of the cerebellum is a nonspecific binding. The self-blockade result demonstrated that [^{125}I]**5** was specific to the brain regions that are rich in α7-nAChRs. In order to confirm the selectivity of [^{125}I]**5**, blockade studies with the homogeneous nAChR

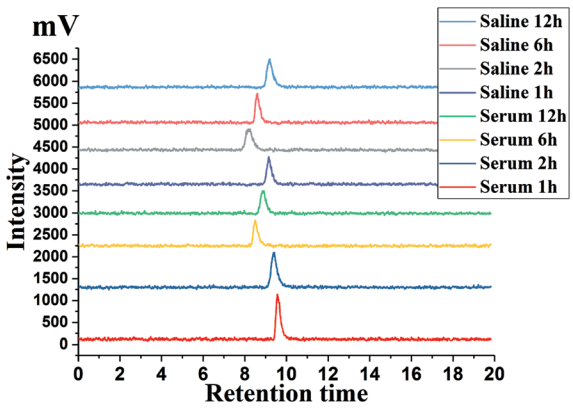

Fig. 3 HPLC chromatograms of [^{125}I]**5** in fetal bovine serum and saline.

Table 2 Biodistribution of [^{125}I]**5** in the Kunming mice (female 1, 18–22 g)[a]

Organs	Time		
	30 min	60 min	120 min
Blood	0.9 ± 0.4	0.9 ± 0.3	0.5 ± 0.2
Brain	7.5 ± 0.9	4.6 ± 0.5	2.8 ± 0.3
Thyroid[b]	1.1 ± 0.2	2.0 ± 0.2	4.5 ± 0.4
Heart	3.3 ± 0.9	2.9 ± 0.4	2.3 ± 0.2
Liver	16.2 ± 1.3	12.0 ± 1.2	8.5 ± 0.5
Spleen	11.0 ± 0.9	7.6 ± 0.6	6.5 ± 1.0
Lungs	21.9 ± 2.5	19.7 ± 2.3	8.4 ± 0.9
Kidney	12.0 ± 1.4	7.4 ± 1.0	5.3 ± 0.6
Muscle	3.9 ± 0.4	2.4 ± 0.4	2.4 ± 0.5
Bone	4.9 ± 0.6	4.6 ± 0.6	3.7 ± 0.5
Intestine	3.4 ± 0.4	5.3 ± 0.6	5.5 ± 0.5
Stomach	4.5 ± 0.6	5.2 ± 0.9	5.9 ± 0.5
Brain/blood	8.3	5.1	5.6

[a] Data are expressed as the percentage of injected dose per gram (% ID g^{-1}), mean ± SD, n = 3. [b] Data are expressed as the percentage of injected dose (% ID), mean ± SD, n = 3.

ligands were performed under the same physiological conditions.

The independent experiments of the blockade studies were conducted for the purpose of determining the specificity of the studied radiotracer to α7-nAChRs over α4β2-nAChRs and 5-HT_3 receptors. The three blocking agents were pre-intravenous/subcutaneous injected before the administration of [^{125}I]**5**. SSR180711, a selective α7-nAChR partial agonist with a good affinity, was chosen to study *in vivo* selectivity.[38] For the α4β2-nAChRs and 5-HT_3 receptors, cytisine and ondansetron were chosen as blocking agents, respectively.[39,40] All the three blocking agents were pre-injected 15 min before the injection of the radiotracer. The non-blocking group was pre-injected with saline to avoid interferences. The mice were sacrificed at 45 min of post-

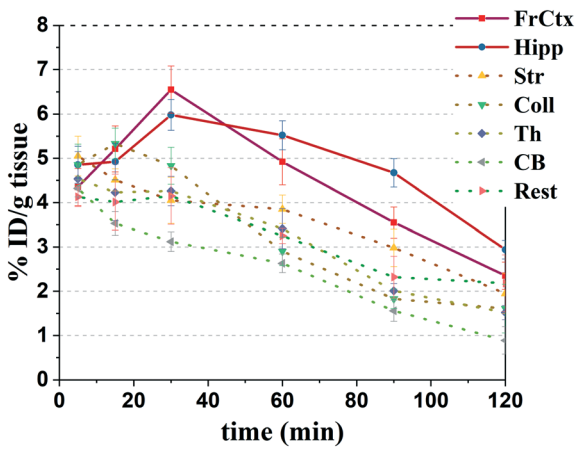

Fig. 4 Biodistribution of [^{125}I]**5** in the cerebral regions of the mice. The data are expressed as the percentage of injected dose per gram (% ID g^{-1}), mean ± SD, n = 3. Abbreviations: FrCtx, frontal cortex; Hipp, hippocampus; Str, striatum; Coll, superior and inferior colliculi; Th, thalamus; CB, cerebellum; Rest, the rest of the brain.

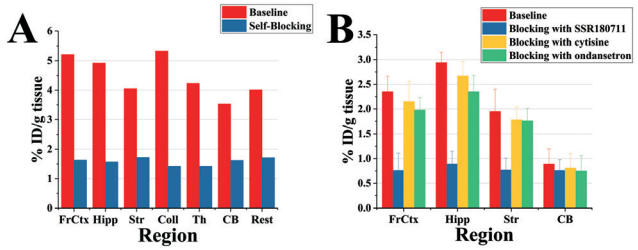

Fig. 5 Blockade studies of [^{125}I]**5**. (A) Self-blocking and (B) blocking with selective α7-nAChR, α4β2-nAChR and 5-HT_3 ligands in the mice. Abbreviations: FrCtx, frontal cortex; Hipp, hippocampus; Str, striatum; Coll, superior and inferior colliculi; Th, thalamus; CB, cerebellum. Rest, the rest of the brain.

injection of the radiotracer and brain tissues were harvested. As shown in Fig. 5B, the SSR180711 blocking group suffered an obvious reduction of radioactivity and the inhibitor ratio was more than 50%, which suggests that [^{125}I]**5** was specific to α7-nAChRs. As for the cytisine and ondansetron blocking groups, the radioactivity accumulation of the front cortex, hippocampus and striatum was hardly reduced. The inhibitor ratio of the two homologous receptors was less than 15%, which demonstrates that [^{125}I]**5** was specific to α7-nAChRs *versus* α4β2 subtypes and 5-HT_3 receptors. In addition, the accumulation of radioactivity in the cerebellum was not influenced by all the blocking agents, which demonstrated that [^{125}I]**5** in the cerebellum was a nonspecific binding.

Ex vivo autoradiography

Blockade studies showed that [^{125}I]**5** has good selectivity and specificity, and to further confirm the binding ability and specificity of [^{125}I]**5** intuitively, *ex vivo* autoradiography on living mice was performed. The results were cross-referenced to mouse brain atlases.[41] As shown in Fig. 6, radioiodinated tracer [^{125}I]**5** exhibited intensive labeling and showed strong radioactive accumulations in the front cerebral cortex, hippocampus, thalamus, and striatum, as

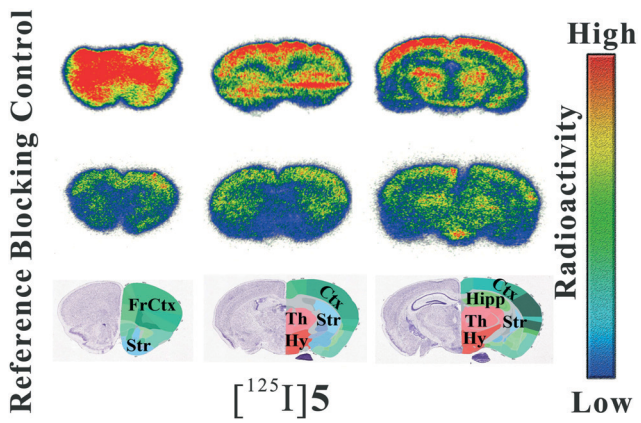

Fig. 6 *Ex vivo* autoradiography of [^{125}I]**5** on the mice.

well as hypothalamus, where α7-nAChRs were highly expressed. Moreover, SSR180711 was used as the blocker to form an inhibiting group. As shown in the figure, [^{125}I]**5** was significantly blocked in the Kunming mice by SSR180711 and the uptakes of all the regions suffered obvious reductions. [^{125}I]**5** showed little unexpected radioactive accumulation and an obvious specific labelling of α7-nAChRs, which proved that it has a good ability for imaging α7-nAChRs.

In vivo SPECT/CT imaging on the Kunming mice

Dynamic SPECT/CT studies of [^{125}I]**5** were further performed on the mice. The mice were anesthetized with isoflurane followed by the intravenous injection of radioiodinated probes (0.1 mL, 80 μCi, 2.96 MBq). Dynamics SPECT/CT was conducted consecutively for 60 min. Moreover, two more static scanning tests (90 min and 120 min of post-injection) have been also performed to study internal retention and metabolism. As shown in Fig. 7A, significant radioactive accumulation was observed post-injection. The mice cerebral regions had an obvious uptake, which is in agreement with the studies discussed above. Slight deiodination was observed during the studies after 30 min, but was in the acceptable limits. [^{125}I]**5** has good cerebral retention and moderate washout in the mice brain. The radioactivity concentration was basically cleared after 120 min. The imaging results are well consistent with the biodistribution data and further proved that radioiodinated [^{125}I]**5** has good dynamic properties in the mice brain.

To further ensure the blockade results, a blocking agent was also used in the study. The mice were pre-injected with SSR180711 (1 mg kg^{-1}) 15 min before the injection of the radiotracer. As shown in Fig. 7B, significant blockade of cerebral uptakes were observed at 30 min and 60 min of post-injection. Taken together, the blocking imaging study, in combination with the dynamics SPECT/CT studies and experiments *in vivo*/*vitro* discussed above, illustrated that radioiodinated **5** was specific and selective to rodent α7-nAChRs. With the good *in vitro*/*vivo* properties of [^{125}I]**5**, it could be an excellent choice for imaging human α7-nAChRs.

Docking study

For purpose of elucidating the binding modes of α7-nAChRs with the series ligands, docking studies were performed using Glide 6.7.[42–44] We chose **3**, **5**, **12**, **13**, **16**, and **18** together with the previously reported compounds ASEM, iodo-ASEM and **DBT-10** hoping to reveal the binding modes of the dibenzo[*b*,*d*]thiophendioxide and 9*H*-fluoren-9-one derivatives. The studied ligands were successfully docked into the binding pockets and the docking poses of iodo-ASEM and **5** are shown in Fig. 8. The docking results revealed that the main interactions of the chosen compounds with α7-nAChR were dominated by the heterocyclic nitrogen groups. The docking poses of the two series of compounds were quite

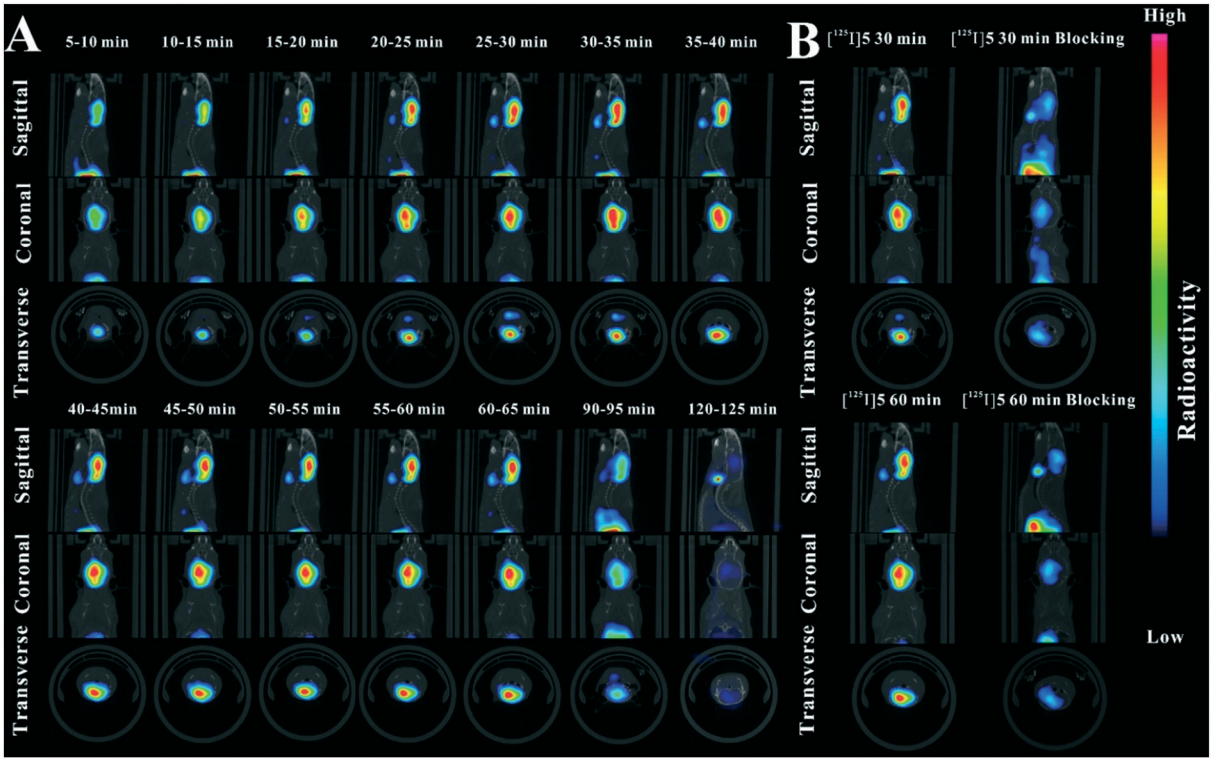

Fig. 7 Dynamic micro-SPECT/CT studies of radiotracers on the Kunming mice (female, 18–22 g). (A) Dynamic micro-SPECT/CT images of [^{125}I]**5**. (B) Micro-SPECT/CT blockade studies of [^{125}I]**5**.

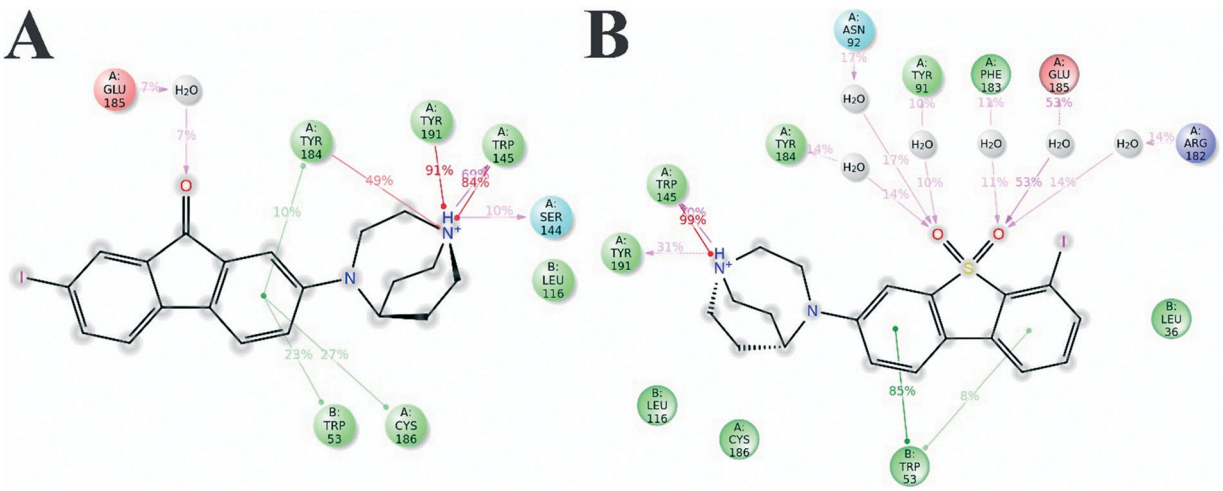

Fig. 8 Binding modes of the ligands in the pockets of α7-nAChRs (PDB code: 3SQ6). (A) Binding contacts during MD simulations of **5** in the active sites of α7-nAChRs. (B) Binding contacts during MD simulations of iodo-ASEM in the active sites of α7-nAChRs.

similar, which illustrated that the 3D geometry of 1,4-diazobicylco[3.2.2]nonane groups may play a vital role in the binding mechanism. For the studied two series of derivatives, a strong H-bond was observed between the protonated secondary/tertiary amine of the nitrogen heterocyclic ring and Trp145. Besides, moderate H-bonds were observed between the oxygen atoms on the sulfonyl/ketone group. Two π–cation interactions between the protonated nitrogen atom and Tyr184/Tyr191 were observed simultaneously. Additionally, a π–π stacking was found between the benzo groups from the basic structure of the two series and Trp53. Interestingly, the π-cations between the protonated nitrogen atom on 4-methylpiperazin-yl and Tyr184 were not found, which may explain the reason why **12** and **16** have lower affinities than **13** and **18**. The predicted binding models demonstrated that among all the α7-nAChR ligands, the heterocyclic nitrogen groups were crucial for the binding mechanism.

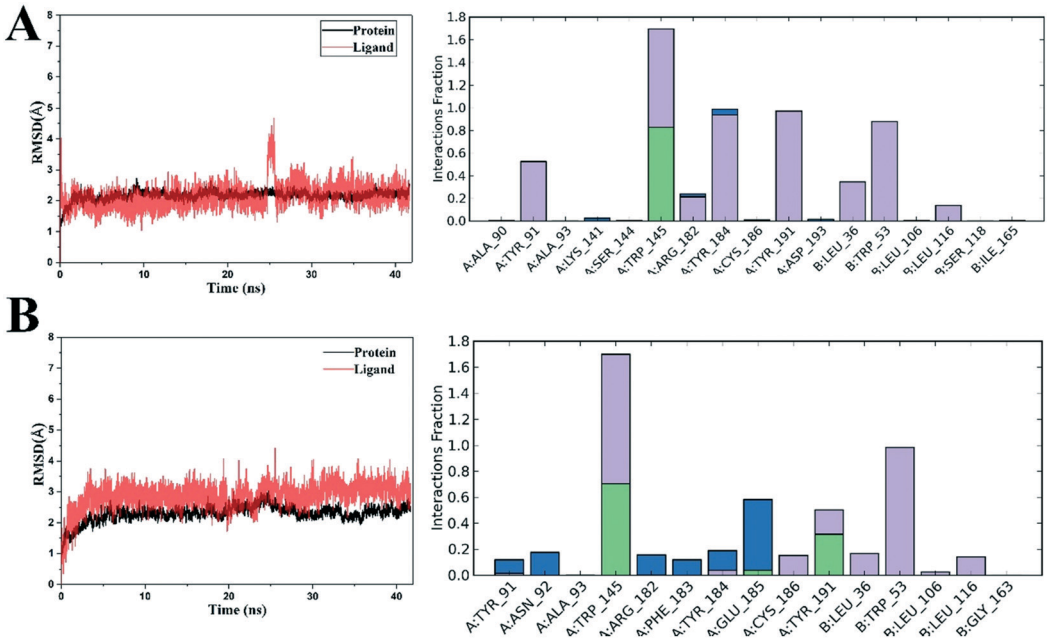

Fig. 9 The RMSDs and interactions of the simulated ligand–α7-nAChR complex backbones and ligand atoms. (A) RMSD and interactions of **5**–α7-nAChR complex. (B) RMSD and interactions of iodo-ASEM–α7-nAChR complex.

Molecular dynamics simulations

Docking studies showed us a feature of the ligands and α7-nAChRs in a static and relatively rigid environment. To further reveal the behaviour of the complexes taking the protein flexibility into account, 40 ns molecular dynamics studies for each complex were conducted in explicit aqueous solution using Desmond 4.2.[45,46] Iodo-ASEM and **5** was chosen to conduct the studies. The RMSD of each system was calculated and analysed to explore their dynamic stability and ensure the rationality of the sampling method.

The RMSDs of the initial structures of proteins and ligands are shown in Fig. 9. The protein–ligand contacts of the systems were also monitored as shown in Fig. 8 and 9. As can be seen in the figure, the two complexes had an initial increase of RMSD at first, which was probably due to the relaxation of the solvated complexes. The studied two complexes showed smooth motion till the end of the simulations and found fluctuations less than 3 Å. The ligand RMSDs that was fitted on the proteins were all smooth likewise, indicating that they all have good binding stability in a dynamic environment. The ligand RDSM of complex **5**–α7-nAChR showed the highest value of more than 4.5 Å, indicating that **5** has a relatively moderate binding affinity towards α7-nAChRs. A sudden fluctuation was found during the simulations, indicating that the bond rotation of **5** may exist. The main backbone residues of the proteins were stable to have low RMSF values during the simulations, indicating less fluctuations of the α7-nAChR protein. For the two ligands, a strong H-bond (backbone acceptor) between Trp145 and the protonated tertiary amine of the nitrogen heterocyclic ring was maintained during the simulations. In addition, another several H-bonds between Glu185, Arg182, Asn92, Tyr184 and a sulfonic base were found in the iodo-ASEM–α7-nAChR complexes. As for the **5**–α7-nAChR complexes, moderate H-bonds were found between the oxygen atom on the ketone group and Glu185 which could be the reason why the 9-fluorenone derivatives exhibited moderate affinity than dibenzo[*b*,*d*]thiophene 5,5-dioxide substituendum. The hydrophobic contacts of the two complexes were more consistent. The hydrophobic contacts between Trp53 and the aromatic rings were found during the simulations. As it's known, H-bonds dominate the ligand binding and hydrophobic interaction is the driving force of binding, they all played important roles in ligand–α7-nAChR binding. To sum up, the stabilizations were achieved from both the H-bonds and π–π stacking hydrophobic contacts, which made the two ligands exhibit high binding affinities to α7-nAChRs. The results of molecular dynamics studies are in good agreement with the assay results and will be a help for further structure-based modifications.

Conclusions

In this paper, a series of 9*H*-fluoren-9-one derivatives with high affinities and selectivity have been synthesized and evaluated for the SPECT/CT imaging of α7-nAChRs. Among the different nitrogen heterocyclic derivatives, *meta*-iodine substituted 9-fluorenone **5** with a high α7-nAChR affinity (K_i = 9.3 ± 0.4 nM) and selectivity *versus* homologous subtypes was radiolabeled with ^{125}I.

[^{125}I]**5** has a good *in vitro* stability and a good blood brain permeability. Furthermore, cerebral biodistribution studies, blocking studies, *ex vivo* autoradiography and micro-SPECT/

CT imaging in mice confirmed the good *in vivo* pharmacokinetic properties. Additionally, docking studies and MD simulations were performed to reveal the binding mechanisms and differences in potency of the studied compounds towards α7-nAChRs.

To sum up, [^{125}I]**5** exhibits excellent properties to study α7-nAChRs *in vitro*/*vivo*. Therefore, **5** may serve as a potential SPECT/CT radiotracer in quantifying α7-nAChRs. Further studies of **5** labelled with ^{123}I are ongoing.

Ethics

All animal studies were carried out in accordance with the Regulations on Laboratory Animals of Beijing Municipality and all procedures were carried out in compliance with the Guidelines for Care and Use of Laboratory Animals of Beijing Normal University and approved by the Animal Ethics Committee of Beijing Normal University.

The fetal bovine serum was obtained from Beijing InnoChem Science & Technology Co., Ltd (Beijing China), in compliance with the regulations mentioned above.

Conflicts of interest

There are no conflicts to declare.

Acknowledgements

This work was supported by the National Major Scientific and Technological Special Project for "Significant New Drugs Development" (Grant No. 2014ZX09507007-001 and 2014ZX09507007-003) and the National Natural Science Foundation of China (Grant No. 21771022 and U1804188). We also thank the Tianjin Institute of Pharmaceutical Research (Tianjin, China) for providing help in the use of the Maestro (Shrödinger, LLC, Portland, OR) software package.

Notes and references

1 R. J. Lukas, J. P. Changeux, N. Le Novere, E. X. Albuquerque, D. J. Balfour, D. K. Berg, D. Bertrand, V. A. Chiappinelli, P. B. Clarke, A. C. Collins, J. A. Dani, S. R. Grady, K. J. Kellar, J. M. Lindstrom, M. J. Marks, M. Quik, P. W. Taylor and S. Wonnacott, *Pharmacol. Rev.*, 1999, **51**, 397.
2 C. Gotti, M. Zoli and F. Clementi, *Trends Pharmacol. Sci.*, 2006, **27**, 482.
3 C. Gotti and F. Clementi, *Prog. Neurobiol.*, 2004, **74**, 363.
4 A. R. Davies, D. J. Hardick, I. S. Blagbrough, B. V. Potter, A. J. Wolstenholme and S. Wonnacott, *Neuropharmacology*, 1999, **38**, 679.
5 K. Murakami, Y. Ishikawa and F. Sato, *Neuroscience*, 2013, **252**, 443.
6 G. Sharma and S. Vijayaraghavan, *Proc. Natl. Acad. Sci. U. S. A.*, 2001, **98**, 4148.
7 T. Teaktong, A. Graham, J. Court, R. Perry, E. Jaros, M. Johnson, R. Hall and E. Perry, *Glia*, 2003, **41**, 207.
8 R. De Simone, M. A. Ajmone-Cat, D. Carnevale and L. Minghetti, *J. Neuroinflammation*, 2005, **2**, 4.
9 G. Sharma and S. Vijayaraghavan, *J. Neurobiol.*, 2002, **53**, 524.
10 B. T. Hawkins, R. D. Egleton and T. P. Davis, *Am. J. Physiol.*, 2005, **289**, H212.
11 J. W. Young and M. A. Geyer, *Biochem. Pharmacol.*, 2013, **86**, 1122.
12 K. G. Ma and Y. H. Qian, *Neuropeptides*, 2019, **73**, 96.
13 M. S. Thomsen, A. Weyn and J. D. Mikkelsen, *Bipolar Disord.*, 2011, **13**, 701.
14 S. L. Verbois, S. W. Scheff and J. R. Pauly, *Neuropharmacology*, 2003, **44**, 224.
15 S. Sydserff, E. J. Sutton, D. Song, M. C. Quirk, C. Maciag, C. Li, G. Jonak, D. Gurley, J. C. Gordon, E. P. Christian, J. J. Doherty, T. Hudzik, E. Johnson, L. Mrzljak, T. Piser, G. N. Smagin, Y. Wang, D. Widzowski and J. S. Smith, *Biochem. Pharmacol.*, 2009, **78**, 880.
16 S. A. Castner, G. N. Smagin, T. M. Piser, Y. Wang, J. S. Smith, E. P. Christian, L. Mrzljak and G. V. Williams, *Biol. Psychiatry*, 2011, **69**, 12.
17 R. Tatsumi, M. Fujio, S. Takanashi, A. Numata, J. Katayama, H. Satoh, Y. Shiigi, J. Maeda, M. Kuriyama, T. Horikawa, T. Murozono, K. Hashimoto and H. Tanaka, *J. Med. Chem.*, 2006, **49**, 4374.
18 H. R. Parri, C. M. Hernandez and K. T. Dineley, *Biochem. Pharmacol.*, 2011, **82**, 931.
19 W. J. de Jonge and L. Ulloa, *Br. J. Pharmacol.*, 2007, **151**, 915.
20 M. A. van Maanen, S. P. Stoof, E. P. van der Zanden, W. J. de Jonge, R. A. Janssen, D. F. Fischer, N. Vandeghinste, R. Brys, M. J. Vervoordeldonk and P. P. Tak, *Arthritis Rheum.*, 2009, **60**, 1272.
21 A. Nordberg, *Biol. Psychiatry*, 2001, **49**, 200.
22 E. Brai, S. Stuart, A. S. Badin and S. A. Greenfield, *Front. Cell. Neurosci.*, 2017, **11**, 291.
23 H. Kitagawa, T. Takenouchi, R. Azuma, K. A. Wesnes, W. G. Kramer, D. E. Clody and A. L. Burnett, *Neuropsychopharmacology*, 2003, **28**, 542.
24 D. Walling, S. R. Marder, J. Kane, W. W. Fleischhacker, R. S. Keefe, D. A. Hosford, C. Dvergsten, A. C. Segreti, J. S. Beaver, S. M. Toler, J. E. Jett and G. C. Dunbar, *Schizophr. Bull.*, 2016, **42**, 335.
25 W. J. Deardorff, A. Shobassy and G. T. Grossberg, *Expert Rev. Neurother.*, 2015, **15**, 7.
26 A. S. Lewis, G. I. van Schalkwyk and M. H. Bloch, *Prog. Neuro-Psychopharmacol. Biol. Psychiatry*, 2017, **75**, 45.
27 T. L. Wallace and D. Bertrand, *Int. Rev. Neurobiol.*, 2015, **124**, 79.
28 K. Hashimoto, S. Nishiyama, H. Ohba, M. Matsuo, T. Kobashi, M. Takahagi, M. Iyo, T. Kitashoji and H. Tsukada, *PLoS One*, 2008, **3**, e3231.
29 H. T. Ravert, P. Dorff, C. A. Foss, R. C. Mease, H. Fan, C. R. Holmquist, E. Phillips, D. J. McCarthy, J. R. Heys, D. P. Holt, Y. Wang, C. J. Endres, R. F. Dannals and M. G. Pomper, *Nucl. Med. Biol.*, 2013, **40**, 731.
30 Y. Gao, K. J. Kellar, R. P. Yasuda, T. Tran, Y. Xiao, R. F. Dannals and A. G. Horti, *J. Med. Chem.*, 2013, **56**, 7574.

31 S. Wang, Y. Fang, H. Wang, H. Gao, G. Jiang, J. Liu, Q. Xue, Y. Qi, M. Cao, B. Qiang and H. Zhang, *Eur. J. Med. Chem.*, 2018, **159**, 255.
32 R. Teodoro, M. Scheunemann, B. Wenzel, D. Peters, W. Deuther-Conrad and P. Brust, *Bioorg. Med. Chem. Lett.*, 2018, **28**, 1471.
33 Y. Gao, R. C. Mease, T. T. Olson, K. J. Kellar, R. F. Dannals, M. G. Pomper and A. G. Horti, *Nucl. Med. Biol.*, 2015, **42**, 488.
34 S. Wonnacott, *J. Neurochem.*, 1986, **47**(6), 1706–1712.
35 A. R. Davies, D. J. Hardick, I. S. Blagbrough, B. V. Potter, A. J. Wolstenholme and S. Wonnacott, *Neuropharmacology*, 1999, **38**(5), 679–690.
36 P. Whiteaker, A. R. Davies, M. J. Marks, I. S. Blagbrough, B. V. Potter, A. J. Wolstenholme, A. C. Collins and S. Wonnacott, *Eur. J. Neurosci.*, 1999, **11**, 2689.
37 L. A. Pabreza, S. Dhawan and K. J. Kellar, *Mol. Pharmacol.*, 1991, **39**(1), 9–12.
38 B. Biton, O. E. Bergis, F. Galli, A. Nedelec, A. W. Lochead, S. Jegham, D. Godet, C. Lanneau, R. Santamaria, F. Chesney, J. Leonardon, P. Granger, M. W. Debono, G. A. Bohme, F. Sgard, F. Besnard, D. Graham, A. Coste, A. Oblin, O. Curet, X. Vige, C. Voltz, L. Rouquier, J. Souilhac, V. Santucci, C. Gueudet, D. Francon, R. Steinberg, G. Griebel, F. Oury-Donat, P. George, P. Avenet and B. Scatton, *Neuropsychopharmacology*, 2007, **32**, 1.
39 H. Rollema, A. Shrikhande, K. M. Ward, F. R. Tingley, J. W. Coe, B. T. O'Neill, E. Tseng, E. Q. Wang, R. J. Mather, R. S. Hurst, K. E. Williams, M. de Vries, T. Cremers, S. Bertrand and D. Bertrand, *Br. J. Pharmacol.*, 2010, **160**, 334.
40 J. H. Ye, R. Ponnudurai and R. Schaefer, *CNS Drug Rev.*, 2001, **7**, 199.
41 *2004 Allen Institute for Brain Science*, Allen Mouse Brain Atlas, Available from: http://mouse.brain-map.org/.
42 Schrodinger, Inc., 101 SW Main Street, Suite 1300, Portland, OR 97204, Accelrys Inc., San Diego, CA, 2006; Glide, version 6.7, Schrödinger, LLC, New York, 2015.
43 R. A. Friesner, J. L. Banks, R. B. Murphy, T. A. Halgren, J. J. Klicic, D. T. Mainz, M. P. Repasky, E. H. Knoll, M. Shelley, J. K. Perry, D. E. Shaw, P. Francis and P. S. Shenkin, *J. Med. Chem.*, 2004, **47**, 1739.
44 T. A. Halgren, R. B. Murphy, R. A. Friesner, H. S. Beard, L. L. Frye, W. T. Pollard and J. L. Banks, *J. Med. Chem.*, 2004, **47**, 1750.
45 Desmond, version 4.2, Schrödinger, LLC, New York, 2015.
46 K. Bowers, E. Chow, X. Huageng, R. O. Dror, M. P. Eastwood, B. Gregersen, J. Klepeis, I. Kolossváry, M. A. Moraes, F. D. Sacerdoti, J. Salmon, Y. Shan and D. E. Shaw, Scalable Algorithms for Molecular Dynamics Simulations on Commodity Clusters, SC 2006 Conference, Proceedings of the ACM/IEEE. ACM.

